Thermodynamic assessment of the Cr–Si binary system

Authors: Kazushige Ioroi[1], Ikuo Ohnuma[2], Xiao Xu[1], Ryosuke Kainuma[1], Toshihiro Omori[1]*

Affiliations:

[1]Department of Materials Science, Graduate School of Engineering, Tohoku University, 6-6-02 Aoba-yama, Sendai 980-8579, Japan

[2]Research Center for Structural Materials, National Institute for Materials Science (NIMS), Tsukuba, 305-0047, Japan

*Corresponding author. Email: omori@material.tohoku.ac.jp

Abstract

A thermodynamic evaluation of the Cr–Si system was performed concerning the latest experimental phase diagram and with the aid of first-principles calculations. The thermodynamic parameters for the Gibbs energy of pure Cr were modified based on the new experimental value of 1861 °C for the melting point of pure Cr, which was previously reported as 1907 °C in the SGTE database. The Gibbs energy descriptions of the Cr_3Si and Cr_5Si_3 phases were revised using $Cr_3(Cr,Si)$- and $(Cr,Si)_5Si_3$-type two-sublattice models to reproduce the latest experimental results of their solubility composition ranges, that is, Cr_3Si extending toward the Cr-rich side and Cr_5Si_3 extending toward the Si-rich side from the stoichiometry. The CrSi and $CrSi_2$ phases were considered line compounds with no solubility range, and the solubility of Cr in the Si phase was ignored. A set of self-consistent thermodynamic parameters for the Cr–Si system was obtained using the CALPHAD technique. The phase diagrams calculated using the optimized parameters showed reasonable agreement with the latest phase equilibrium data and thermodynamic property data in the literature, including the enthalpy of mixing, formation enthalpy, and chemical potential diagrams of Cr and Si in the equilibrium phases.

1. Introduction

Cr–Si alloys possess attractive properties such as high specific strength, excellent oxidation and nitridation resistance, and high thermal stability, making them candidates for advanced structural and functional materials. For high-temperature structural material applications, Cr–Si alloys with high Cr concentrations have shown promising results. Cr–13at.%Si alloys with a eutectic microstructure consisting of a body-centered cubic (bcc)-Cr solid solution and Cr_3Si phases exhibit higher specific strength at elevated temperatures than Ni-based superalloys [1]. Due to the formation of Cr_3Si layers on the substance, Cr-*x*Si alloys with a Cr_3Si phase (x = 16, 19, and 25 at.%) exhibit excellent resistance to oxidation and nitridation after 1000 h of exposure at 1200 °C in synthetic air [2]. The addition of ternary elements Ge, Mo, and V can improve the creep resistance and toughness of Cr–Si alloys [3–6]. Thermogravimetric experiments at 1200 °C for 100 h in synthetic air have shown that the oxidation resistance of Cr–Si alloys improves when 2 at.% Si is replaced by Ge, Mo, or Pt [7,8].

The $CrSi_2$ compound phase can be a promising candidate for thermoelectric material applications because of its excellent electrical conductivity (σ) and Seebeck coefficient. For example, bulk $CrSi_2$ has a Seebeck coefficient of approximately 100 μV/K electrical resistivity ($\rho=1/\sigma$) on the order of 10^{-3} Ω·cm [12], and high thermal stability up to 1000 K in air [13]. However, the thermal conductivity of $CrSi_2$ at room temperature is rather high (approximately 10 W/m·K), which adversely affects its thermoelectric performance. To improve the thermoelectric properties of $CrSi_2$, attempts have been made to combine nanoscale and porous structures [14,15] and to dope it with impurities such as Al, V, Mo, and Mn [12,16–20].

Understanding the phase equilibria of Cr–Si system is important for the development of related materials. Recently, we experimentally determined the melting point of pure Cr and phase equilibria in the Cr–Si binary system, revealing some noticeable improvements [21]. Accurate assessment and revision of thermodynamic parameters to reflect these improvements are crucial for the design of Cr–Si alloys and for the development of a thermodynamic database of Cr-based alloy systems. Therefore, the present study aimed to evaluate the thermodynamic parameters of the Cr–Si binary system using the CALPHAD (Calculation of Phase Diagrams) method based on the latest experimental data.

2. Literature review

2.1. Phase diagram information

The latest thermodynamic assessment of the Cr–Si phase diagram was proposed by Cui and Jung [22] in 2017, based on experimental data in the literature [23–30] marked by gray symbols in Fig. 1. The phase diagram calculated using their thermodynamic parameters [22] is shown in Fig. 1 by grey lines, where the latest experimental data reported in 2022 [21] are plotted by black symbols; thus, a discrepancy is observed between them. A summary of the crystal structure information for all solution phases and stable compounds in the Cr–Si system [31–36] is provided in Table 1.

The phase equilibrium data over the entire composition range were investigated by Chang [24] and Svechnikov et al. [25]. Chang [24] measured the phase equilibria using the Pirani method, differential thermal analysis (DTA), X-ray diffraction (XRD), and metallographic analysis. Sevchnikov et al. [25] measured the phase equilibria over the entire composition range using XRD, metallographic analysis, and DTA. The phase boundaries of the $CrSi_2$ single-phase region were proposed by Voronov et al. [26], Dubrovskaya and Gel'd [27], and Dudkin and Kuznetsova [28] using electrical conductivity measurements. Pyatkova et al. [29] and Jurisch and Behr [30] reported on the homogeneity range of the Cr_3Si phase using XRD and metallographic analyses. Du and Schuster [23] revised the liquidus curves and invariant temperatures of Si-rich alloys by using DTA. The equilibrium compositions of the bcc-Cr solid solution and Cr_3Si phases at 1200 and 1350 °C were also determined by Pfizenmaier [37] using EDS analysis.

Owing to the lack of experimental data for critical thermodynamic evaluation, we have experimentally re-examined the phase equilibria of the Cr–Si system at elevated temperatures from 1200 to 1600 °C over the entire composition range [21]. Heat treatment above 1500 °C was carried out in a meticulously designed high-frequency induction furnace, and the temperature accuracy was carefully assessed using a two-color pyrometer.

As Fig. 1 shows, our study [21] achieved the following significant improvements regarding the phase diagram compared to previous studies: (1) the melting point of pure Cr was revised to be 1861 ± 3 °C; (2) the Cr_3Si single-phase region extends from the stoichiometric composition to the Cr-rich side rather than the Si-rich side [22]; (3) the Cr_5Si_3 phase has a considerable solubility range which extends toward the Si-rich side; (4) there is no α/β transformation in the Cr_5Si_3 phase; (5) the invariant reaction related to the formation of Cr_3Si and Cr_5Si_3 phases is not the peritectic reaction (Liquid + Cr_3Si = Cr_5Si_3), but the eutectic one (Liquid = Cr_3Si + Cr_5Si_3); (6) the $CrSi_2$ phase has little compositional range of solubility.

2.2. Thermodynamic information

2.2.1 Formation enthalpy of intermetallic compound (IMC) phases and mixing enthalpy of liquid phase

The formation enthalpies of the Cr–Si compounds, Cr_3Si, Cr_5Si_3, CrSi, and $CrSi_2$, were determined by calorimetry [38,45,46] or derived from measurements of the electromotive force (EMF) [39–41] and vapor pressure [42]. Golutvin and Liang [45] measured these properties using bomb calorimetry at 25 °C. Meschel and Kleppa [38] measured the formation enthalpies of the Cr_3Si, Cr_5Si_3, and CrSi phases using high-temperature direct-synthesis calorimetry at 1200 ± 2 °C. The formation enthalpy of the $CrSi_2$ phase was investigated by Topor and Kleppa [46] using high-temperature solute–solvent drop calorimetry at 1127 °C. Additionally, formation enthalpies of those IMC phases at 25 °C were estimated through extrapolation of data reported by Eremenko et al. [39,40] and Lukashenko et al. [41] using EMF measurements, as well as by Chart [42] using the Knudsen-effusion vapor-pressure method.

Esin et al. [47] measured the partial and integral mixing enthalpies of liquid Cr–Si alloys up to 68 at.% Cr at 1723 °C using a high-temperature calorimeter.

2.2.2 Chemical potential of Cr and Si in two-phase alloys

The chemical potential of Cr in the two-phase alloys was estimated by Eremenko et al. [39,40] and Lukashenko et al. [41]. They investigated the partial Gibbs energies of Cr in Cr–Si alloys in the temperature range of 680 to 860 °C using EMF measurement. The activities of Cr and Si were estimated by Chart [42], Riegert et al. [43], and Myers et al. [44]. Chart [42] determined the activities of Si in two-phase alloys by Knudsen-effusion vapor-pressure method, in which the partial pressure of SiO vapor generated by the reaction of a Cr–Si alloy with SiO_2 was measured at temperatures between 1050 and 1438 °C. Using the same technique, Riegert et al. [43] measured the activity of Cr in the liquid phase at 1627 °C in the composition range from 28.7 to 55.8 at.% Cr. Myers et al. [44] also measured the activities of Cr and Si in two-phase alloys at 1227 °C.

2.2.3 Specific heat of IMC phases

The specific heat of the stable phases have been reported by Golutvin and Liang [45], Kalishevich et al. [48–50], Pan et al. [51], and Surikov et al. [52]. Golutvin and Liang [45] measured the specific heat of the Cr_3Si, Cr_5Si_3, CrSi, and $CrSi_2$ phases in the temperature range of 25–600 °C using bomb calorimetry. Kalishevich et al. [48–50] used an adiabatic calorimeter to measure the specific heat of Cr, Cr_3Si, Cr_5Si_3, CrSi, $CrSi_2$, and Si at low temperatures from -219 to 27 °C and the enthalpy of melting of the Cr_5Si_3, CrSi, and $CrSi_2$ phases at high temperature up to 1727 °C. In addition, the specific heat of the Cr_3Si phase within a temperature range of -267 to 27 °C was measured by Pan et al. [51] and Surikov et al. [52] using an adiabatic calorimeter.

2.3. Thermodynamic calculations

The thermodynamic assessment of the Cr–Si binary system was first published by Coughanowr and Ansara [53] in 1994, where two binary compound phases, Cr_3Si and $CrSi_2$, were modeled as solid solutions with a certain solubility range, whereas the other two phases, Cr_5Si_3 and CrSi, were modeled as stoichiometric compounds. Du and Schuster [23] re-optimized the thermodynamic parameters by

considering the new enthalpy of formation from Meschel and Kleppa [38] and their experimental results on the Si-rich side. They considered the high-temperature β-Cr_5Si_3 phase and applied the model used for Ti_5Si_3 to describe the β-Cr_5Si_3 phase in addition to the low-temperature α-Cr_5Si_3 phase known as the W_5Si_3 structure. Chen et al. [54] revised the thermodynamic parameters based on the assumption that the invariant reaction consisting of the liquid, Cr_3Si, and Cr_5Si_3 phases was peritectic. Recently, Cui and Jung [22] completed a thermodynamic re-assessment by applying a modified quasi-chemical model (MQM) to the liquid phase.

3. Thermodynamic model

3.1. Pure Cr and Si

The Gibbs energies of the stable and metastable structures of pure Cr and Si are taken from the SGTE database constructed by Dinsdale [55]. It should be noted that the melting point of pure Cr accepted in the SGTE database (${}^{\mathrm{SGTE}}T_{\mathrm{m}}^{\mathrm{Cr}}$ =1907 ± 20 °C) is likely overestimated compared to the actual values. In our latest experimental investigation [21], the melting point of pure Cr has been determined to be 1861 ± 3 °C. As a matter of fact, the melting point of 1863 °C has been recommended by Xiong et al. [56], Hultgren et al. [57], and Okamoto et al. [58]. Besides, this is supported by the recent experimental investigations by Rudy and Windisch [59] (1860 ± 6 °C) and Josell et al. [60] (1842 ± 20 °C). Therefore, the melting point of $T_{\mathrm{m}}^{\mathrm{Cr}}$ =1861 °C (2134 K) was used as the revised value for pure Cr in the present work. Accordingly, the lattice stability functions of the liquid Cr were corrected as follows:

$$G_{\mathrm{m}}^{\mathrm{liq.-Cr}} = {}^{\mathrm{SGTE}}G_{\mathrm{m}}^{\mathrm{liq.-Cr}} - 546.1873 + 0.053127\,T - 0.075764 \times 10^{-21}\,T^{7} \ \ (\mathrm{J/mol})$$

$$298.15 \leq \mathrm{T/K} \leq 2134 \qquad (1)$$

and

$$G_{\mathrm{m}}^{\mathrm{liq.-Cr}} = {}^{\mathrm{SGTE}}G_{\mathrm{m}}^{\mathrm{liq.-Cr}} - 448.0401 \ \ (\mathrm{J/mol}) \quad 2134 \leq \mathrm{T/K} \leq 6000 \qquad (2)$$

to lower the melting temperature of pure Cr from 1907 to 1861 °C and to keep the continuity of the lattice stability functions of the liquid Cr at $T_{\mathrm{m}}^{\mathrm{Cr}}(= 2134\ \mathrm{K})$, which becomes the revised boundary temperature of the lattice stability functions of each phase. Concomitantly, that of the bcc-Cr above $T_{\mathrm{m}}^{\mathrm{Cr}}$ was corrected to

$$G_{\mathrm{m}}^{\mathrm{bcc-Cr}} = {}^{\mathrm{SGTE}}G_{\mathrm{m}}^{\mathrm{bcc-Cr}} - 887.16823 + 0.3702\,T + 0.89954 \times 10^{32}\,T^{-9}\ \ (\mathrm{J/mol})$$

$$2134 \leq \mathrm{T/K} \leq 6000 \qquad (3)$$

to maintain the continuity of the lattice stability functions of the bcc-Cr at $T_{\mathrm{m}}^{\mathrm{Cr}}$. The modified thermodynamic parameters of the lattice stability and calculated thermodynamic properties of pure Cr are shown in Table 2 and Fig. 2, respectively. The main change in the new lattice stability of Cr is the lower value of the constant term corresponding to the enthalpy at 0 K in the liquid phase, and the differences in the specific heat and entropy are small in the bcc-Cr and liquid phases.

3.2. Solution phases

The Gibbs energies of the liquid and bcc-Cr solid solution phases are described by the sub-regular solution approximation for substitutional solutions using the following equation:

$$G_{\mathrm{m}}^{\phi} = G_{\mathrm{Cr}}^{\phi}x_{\mathrm{Cr}} + G_{\mathrm{Si}}^{\phi}x_{\mathrm{Si}} + RT(x_{\mathrm{Cr}}\ln x_{\mathrm{Cr}} + x_{\mathrm{Si}}\ln x_{\mathrm{Si}}) + x_{\mathrm{Cr}}x_{\mathrm{Si}}L_{\mathrm{Cr,Si}}^{\phi} + {}^{\mathrm{mag}}G_{\mathrm{m}}^{\phi}, \qquad (4)$$

where G_{Cr}^{ϕ} and G_{Si}^{ϕ} are the Gibbs energies of pure Cr and pure Si, respectively, in the corresponding structure of ϕ; x_{Cr} and x_{Si} are the mole fractions of Cr and Si, respectively; and $L_{\mathrm{Cr,Si}}^{\phi}$ is the interaction parameter, which has a composition dependence in the form of the Redlich–Kister (RK) polynomial [61] described by the following equation:

$$L_{\mathrm{Cr,Si}}^{\phi} = \sum_{i=0}^{n}(x_{\mathrm{Cr}} - x_{\mathrm{Si}})^{i} \cdot {}^{i}L_{\mathrm{Cr,Si}}^{\phi}. \qquad (5)$$

Interaction parameters ${}^{i}L_{\mathrm{Cr,Si}}^{\phi}$ with temperature dependence are evaluated based on the experimental data on phase boundaries and thermodynamic properties. The model of the magnetic contribution to the Gibbs energy formulated by Inden [62,63] - Hillert and Jarl [64] is applied to calculate ${}^{\mathrm{mag}}G_{\mathrm{m}}^{\phi}$ of the bcc-Cr solid solution phase.

3.3. Intermetallic compound phases

Compound energy formalism (CEF) [65] was applied to describe the Gibbs energies of the Cr_3Si and Cr_5Si_3 phases. Based on our latest experimental investigation [21], $(Cr)_3(Cr,Si)$-type two-sublattice model was used for the Cr_3Si phase. The molar Gibbs energy of the Cr_3Si phase using CEF is expressed as follows:

$$G_{\mathrm{m}}^{\mathrm{Cr_3Si}} = y_{\mathrm{Cr}}^{\mathrm{II}} G_{\mathrm{Cr:Cr}}^{\mathrm{Cr_3Si}} + y_{\mathrm{Si}}^{\mathrm{II}} G_{\mathrm{Cr:Si}}^{\mathrm{Cr_3Si}} + RT\left(y_{\mathrm{Cr}}^{\mathrm{II}} \ln y_{\mathrm{Cr}}^{\mathrm{II}} + y_{\mathrm{Si}}^{\mathrm{II}} \ln y_{\mathrm{Si}}^{\mathrm{II}}\right) + y_{\mathrm{Cr}}^{\mathrm{II}} y_{\mathrm{Si}}^{\mathrm{II}} L_{\mathrm{Cr:Cr,Si}}^{\mathrm{Cr_3Si}}, \quad (6)$$

where $y_{\mathrm{Cr}}^{\mathrm{II}}$ and $y_{\mathrm{Si}}^{\mathrm{II}}$ are the site fractions of Cr and Si, respectively, in the second sublattice; $G_{\mathrm{Cr:Cr}}^{\mathrm{Cr_3Si}}$ and $G_{\mathrm{Cr:Si}}^{\mathrm{Cr_3Si}}$ are the Gibbs energies of the corresponding hypothetical pure Cr phase with Cr_3Si structure and the practically stable Cr_3Si phase, respectively; and $L_{\mathrm{Cr:Cr,Si}}^{\mathrm{Cr_3Si}}$ is the interaction parameter between Cr and Si in the second sublattice, where Cr occupies the first sublattice.

The α-Cr_5Si_3 phase has been treated as a stoichiometric compound, and two or three sublattice model was used for the β-Cr_5Si_3 phase in the previous works [22,23,53,54]. However, in the present work, only one Cr_5Si_3 phase (α-Cr_5Si_3) was considered, based on the experimental results that there is no α-Cr_5Si_3/β-Cr_5Si_3 transformation. The Cr_5Si_3 phase has four Wykoff positions, in which there are two inequivalent Wyckoff positions of atoms for Cr and Si sites, respectively. In the present work, a two-sublattice model was used for the Cr_5Si_3 phase by assuming one Wykoff position for Cr and Si, respectively. Applying a simplified thermodynamic model to the Cr_5Si_3 phase has the advantage that it can be easily extended to higher order systems. In our experimental investigation [21], the solubility range of Cr_5Si_3 phase extends only toward the high Si side, indicating that Si atoms occupies the Cr site. Therefore, the $(Cr,Si)_5(Si)_3$-type two-sublattice model was used for the Cr_5Si_3 phase in the present work.

The CrSi and $CrSi_2$ phases were treated as stoichiometric compounds.

3.4. First-principles calculation

The formation energies of the Cr_3Si, Cr_5Si_3, CrSi, and $CrSi_2$ phases at 0 K were estimated by first-principles calculations based on density functional theory (DFT) using the Vienna Ab initio Simulation Package (VASP) [66,67] and the projector augmented wave (PAW) method [68]. The exchange correlation function was treated using the Perdew–Burke–Ernzerhof (PBE) generalized gradient approximation (GGA) approach [69]. Spin polarization was considered in the present calculations. The magnetic ground state of Cr has been reported to be the incommensurate SDW (spin density wave) [70], which makes calculations considering the accurate magnetic structure extremely difficult. Since the incommensurate SDW of Cr is very close to the commensurate one, in this study, we used the perfect antiferromagnetic structure, which is a reasonably suitable model also having been considered in previous literature [71]. Geometry optimization was performed using the conjugate-gradient algorithm, and the structure was considered to converge when the difference in the total energies between the last two iterations was smaller than 0.001 eV/cell. The final self-consistent static calculation was performed using the tetrahedron method with Blöchl corrections [72]. The cut-off energy for the plane waves was set to 400 eV, and the *k*-points for the Brillouin zone integration were confined to 16 × 16 × 16 for cubic Cr, 7 × 7 × 7 for cubic Cr_3Si, 5 × 8 × 8 for tetragonal Cr_5Si_3, 7 × 7 × 7 for cubic CrSi, 9 × 9 × 5 for hexagonal $CrSi_2$, and 10 × 10 × 10 for diamond Si.

The formation energies per one mole of the constituent atoms for Cr_3Si, Cr_5Si_3, CrSi, and $CrSi_2$ structures were computed as follows:

$$\Delta H\left(\mathrm{Cr}_{(1-x)}\mathrm{Si}_x\right) = E\left(\mathrm{Cr}_{(1-x)}\mathrm{Si}_x\right) - (1-x)E(\mathrm{Cr}) - xE(\mathrm{Si}), \quad (7)$$

where $E(\mathrm{Cr})$, $E(\mathrm{Si})$, and $E\left(\mathrm{Cr}_{(1-x)}\mathrm{Si}_x\right)$ are the total energies per one mole of the constituent atoms of bcc-Cr, diamond-Si, and intermetallic compounds, respectively.

4. Results and discussion

The thermodynamic parameters of the Cr–Si system were optimized using the PARROT module implemented in the Thermo-Calc software, which is based on the least-squares method. Optimization

was performed step-by-step to obtain an agreement between the calculated results and the thermodynamic and phase equilibrium data in the literature.

The thermodynamic parameters for the bcc-Cr solid solution and liquid phases were evaluated to reproduce our phase equilibrium data [21] as well as some reported data, including the mixing enthalpy of the liquid phase at 1723 °C measured by Esin et al. [36]. The parameters for the Cr_3Si, Cr_5Si_3, CrSi, and $CrSi_2$ phases were optimized to fit the newly determined phase boundaries shown in Fig. 1, the formation enthalpy of IMC phases at 25 °C, and the chemical potential of Cr (μ_{Cr}) and Si (μ_{Si}) in the equilibrated phases.

Table 3 lists the formation energies calculated in this study and those calculated by Pan et al. [74,75] and Ren [76], as well as those taken from the open databases OQMD (Open Quantum Materials Database), MP (Materials Project), and AFLOW (Automatic FLOW for Materials Discovery). The Cr–Si compounds have been found nonmagnetic except for CrSi, whose total magnetic moment is 1.33 μ_B/unit (8 atoms). The present DFT results were in good agreement with those of previous studies [74–76] except for the formation enthalpy of $CrSi_2$ calculated by Ren et al. [76]. Our results were also consistent with those cited from OQMD and AFLOW, but there were significant discrepancies with the formation energies quorted from MP. Thus, it indicates that MP database has room for improvement. The formation enthalpies of Cr_3Si, Cr_3Cr, Cr_5Si_3, and Si_5Si_3, which are the end members of the corresponding structures $Cr_3(Cr,Si)$ and $(Cr,Si)_5Si_3$, were estimated by first-principles calculations and used as the initial parameters in the present optimization. The final thermodynamic parameters of the Cr–Si binary system are listed in Table 4.

Fig. 3 shows the calculated Cr–Si phase diagram compared with the experimental data from our study [21] and the literature data [23–30,37], in which an overall agreement can be confirmed. Fig. 4 shows the calculated Cr–Si phase diagrams enlarged to focus on (a) the melting point of pure Cr, liquidus, and solidus curves of the Cr solid solution phase, (b) the eutectic reaction of Liquid = Cr_3Si + Cr_5Si_3, and (c) the solubility composition ranges of the Cr_3Si and Cr_5Si_3 phases. As can be seen from these phase diagrams, the calculated phase boundaries adequately reproduced our experimental

data. As Fig. 4(a) shows, large discrepancies between our experimental data and the liquidus and solidus lines starting from the melting point of pure Cr at 1906 °C calculated by Cui and Jung [22] are recognized. However, the melting point of pure Cr was modified to 1861 °C in the present study, which is consistent with the liquidus and solidus temperatures of the Cr solid solution phase. The calculated invariant reaction temperatures are compared with the experimental data [21] in Table 5. Reasonable agreement was obtained between the calculation and experimental data within ±10 °C. In particular, there was a remarkable improvement in the invariant reaction associated with the liquid, Cr_3Si, and Cr_5Si_3 phases. The invariant reaction was evaluated by Chen as the peritectic reaction "Liquid + Cr_3Si = Cr_5Si_3" [54] and by Cui and Jung as the eutectic reaction "Liquid = Cr_3Si + Cr_5Si_3" which has a eutectic composition quite close to the stoichiometry of the Cr_5Si_3 phase (37.5 at.% Si) [22] as shown in Fig. 4(b). In the present evaluation, however, the invariant reaction is revised to be a eutectic one "Liquid = Cr_3Si + Cr_5Si_3" mainly because the congruent melting temperature of the Cr_5Si_3 phase (1690 °C [21]) is clearly higher than the invariant temperature (1665 °C [21]) as shown in Fig. 4(b). The eutectic composition of the liquid phase is estimated to be 35 at.% Si [21]. Fig. 4(c) shows the calculated solubility composition ranges of the Cr_3Si and Cr_5Si_3 phases compared with our experimental data [21]. In a previous evaluation by Cui and Jung [22], the Cr_3Si phase was described using a $(Cr,Si)_3(Cr,Si)$-type sublattice model, and its solubility range was extended from the stoichiometric composition to the Si-rich side. However, according to the latest experimental results, the solubility range of the Cr_3Si phase extends from the stoichiometry of $x_{Si} = 0.25$ only toward the high-Cr side [21], which is well reproduced by applying the $Cr_3(Cr,Si)$-type sublattice in the present calculation. Although the α-Cr_5Si_3 phase was treated as a stoichiometric compound in the previous assessment [22], the application of the $(Cr,Si)_5Si_3$-type sublattice model also reproduced well the solubility range that extends only toward the high Si side [21].

Calculated enthalpies of formation at 25 °C of all the intermetallic compounds are shown in Fig. 5 in comparison with experimental data [38,39–42,45,46] and the DFT calculations [74–76]. The

optimized enthalpies of formation of Cr–Si compounds were in reasonable agreement with the experimental data obtained by Eremenko [39,40] and Lukashenko [41] using EMF measurements.

The enthalpy of mixing for the liquid Cr–Si phase at 1723 °C calculated through the present optimization is shown in Fig. 6 and compared with experimental data measured by Esin et al. [47]. Most of the data were satisfactorily reproduced using the present calculation.

Calculated phase diagrams of the chemical potential of Cr (μ_{Cr}) and Si (μ_{Si}) vs. temperature are shown in Fig. 7(a) and Fig. 7(b), respectively, in comparison with those calculated by Cui and Jung [22] as well as experimental data [39–44]. In these diagrams, the two- and three-phase equilibria are drawn as lines and triple junctions, respectively, and the spaces surrounded by these lines represent the single-phase regions. As shown in Fig. 7(a) and Fig. 7(b), the results calculated in the present study almost accurately reproduced the experimental data [39–44]. In the case of the chemical potential diagram of Cr, the agreement with the experimental data measured by Eremenko was improved compared with the calculation by Cui and Jung [22]. The calculated chemical potential diagram of Si is also in good agreement with the experimental data measured by Chart [42], except for the (Cr) + Cr_3Si two-phase equilibrium. The chemical potential of Si in the Cr–Si alloys was determined by Chart [42] by measuring the vapor pressure of the SiO vapor phase, which should be as pure as possible. He reported that the measured SiO vapor pressure from a high-Cr alloy (85 at.% Cr) showed large errors compared to low-Cr alloys (66, 55, 52, and 40 at.% Cr). This indicates that the presence of Cr vapor as an undesirable impurity in the SiO vapor may have caused experimental difficulties and errors in the Si chemical potential.

Fig. 8 shows the calculated specific heats of the Cr–Si compounds along with experimental data [45,48–52]. Excess specific heat has been introduced into the end members of the Cr–Si compounds to reproduce experimental data as summarized in Table 4. In the previous assessment by Cui and Jung [22], the thermodynamic parameters of the stoichiometric Cr_5Si_3, CrSi, and $CrSi_2$ IMC phases were optimized based on the experimental specific heat data reported by Kalishevich et al. [48–50], whereas those of the Cr_3Si phase were evaluated based on the Neumann–Kopp relation because the

experimental specific heat data at high temperatures were insufficient to determine all coefficients of the Gibbs energy function. In addition, other functions of the α- and β-Cr_5Si_3 phases above 1900 K (1627 °C) were incorporated, presumably to prevent unintended appearance of the stable α- and β-Cr_5Si_3 phases at high temperatures. In the present optimization, the thermodynamic parameters of the stoichiometric Cr–Si compounds evaluated by Cui and Jung [22] were slightly modified to reproduce the relevant phase equilibria so as not to change the calculated specific heat data. The boundary temperature of the functions of the Cr_5Si_3 phase was revised to 1963 K (1690 °C) which was determined to be congruent melting temperature of the Cr_5Si_3 phase by our experimental investigation [21], and the thermodynamic parameters were modified to maintain the continuity of the functions. As a result, the calculated specific heats of the Cr–Si compounds showed good agreement with the experimental data, as shown in Fig. 8.

5. Conclusions

A thermodynamic evaluation of the Cr–Si system was performed using the CALPHAD method over the entire composition range with the aid of first-principles calculations. Compared with previous thermodynamic evaluations, the thermodynamic parameters were revised to reproduce the latest and previous experimental data with the following improvements.

(1) The melting point of pure Cr was revised from the SGTE recommended value of 1907 °C to 1861 °C. Accordingly, the liquidus and solidus curves of the bcc-Cr solid solution phase were significantly modified.

(2) The solubility of Si in the bcc-Cr solid solution phase was modified to lower the Si content.

(3) The sublattice constructions for the Gibbs energy description of the Cr_3Si and Cr_5Si_3 phases were revised to the $Cr_3(Cr,Si)$ and $(Cr,Si)_5Si_3$ models, respectively, which enabled successful calculations of their solubility composition ranges, that is, a Cr-rich extension for Cr_3Si and a Si-rich extension for Cr_5Si_3 from their stoichiometric compositions.

(4) The invariant reaction associated with the Liquid, Cr_3Si, and Cr_5Si_3 phases was revised from the peritectic reaction "Liquid + Cr_5Si_3 = Cr_3Si" to the eutectic one "Liquid = Cr_3Si + Cr_5Si_3".

(5) The calculated thermodynamic properties, including enthalpies of mixing of Cr–Si liquids and enthalpies of formation of Cr–Si intermetallic compounds at 25 °C, are in good agreement with experimental data in the literature. In particular, the agreement between the calculated chemical potentials of Cr (μ_{Cr}) and Si (μ_{Si}) in equilibrium phases and the experimental values from the literature is significantly better than in the previous evaluations, indicating the validity of the thermodynamic parameters optimized in the present study. The calculated specific heats of Cr–Si compounds are in good agreement with the experimental data from the literature.

These thermodynamic parameters are useful for the future development of Cr-based alloys.

Acknowledgments

This study was supported by JSPS KAKENHI Grant Number JP20H00298 and by JPNP20004 subsidized by the New Energy and Industrial Technology Development Organization (NEDO).

References

1. Y. Aono, T. Omori, R. Kainuma, "Microstructure and high-temperature strength in Cr–Si binary alloys," Intermetallics 112 (2019) 106526.
2. A. Soleimani-Dorcheh, and M.C. Galetz, "Oxidation and Nitridation Behavior of Cr–Si Alloys in Air at 1473 K," Oxid Met, 84 (2015) 73–90.
3. S.V. Raj, "A preliminary assessment of the properties of a chromium silicide alloy for aerospace applications," Mater. Sci. Eng. A 192 (1995) 583–589.
4. T.A. Cruse, J.W. Newkirk, "Evaluation of methods to produce tough Cr_3Si based composites," Mater. Sci. Eng. A 239 (1997) 410–418.
5. S.V. Raj, J.D. Whittenberger, B. Zeumer, G. Sauthoff, "Elevated temperature deformation of Cr_3Si alloyed with Mo," Intermetallics 7 (7) (1999) 743–755.

6. P. Pfizenmaier, A.S. Ulrich, M.C. Galetz, U. Glatzel, “Tensile Creep Properties of Cr–Si Alloys at 980 °C in Air—Influence of Ge and Mo Addition,” Metals 11 (2021) 1072.
7. A. Soleimani-Dorcheh, and M.C. Galetz, “Oxidation-Nitridation Mechanism in Eutectic Cr–Silicide Alloy and Its Mitigation by Germanium Alloying,” Oxid Met, 88 (2017) 549–564.
8. A.S. Ulrich, P. Pfizenmaier, A. Solimani, U. Glatzel, M.C. Galetz, “Improving the oxidation resistance of Cr–Si-based alloys by ternary alloying,” Corrosion Science 165 (2020) 108376.
9. M.E. Qader, R. Venkat, R. Kumar, T. Hartmann, P. Ginobbi, N. Newman, R. Singh, “Structural, electrical, and thermoelectric properties of $CrSi_2$ thin films,” Thin Solid Films 545 (2013) 100–105.
10. T. Dasgupta, J. Etourneau, B. Chevalier, S.F. Matar, A.M. Umarji, “Structural, thermal, and electrical properties of $CrSi_2$,” Journal of Applied Physics 103 (2008) 113516.
11. I. Nishida, “The crystal growth and thermoelectric properties of chromium disilicide,” Journal of Materials Science 7 (1972) 1119–1124.
12. I. Nishida, T. Sakata, “Semiconducting properties of pure and Mn-doped Chromium disilicides,” J. Phys. Chem. Solids 39 (1978) 499–505.
13. J. Ma, Y. Gu, L. Shi, L. Chen, Z. Yang, Y. Qian, “Synthesis and thermal stability of nanocrystalline chromium disilicide,” J. Alloy. Comp. 376 (2004) 176–179.
14. S. Karuppaiah, M. Beaudhuin, R. Viennois, “Investigation on the thermoelectric properties of nanostructured $Cr_{1-x}Ti_xSi_2$,” Journal of Solid State Chemistry 199 (2013) 90–95.
15. M. Khalil, A. Moll, M. Godfroy, A. Letrouit-Lebranchu, B. Villeroy, E. Alleno, R. Viennois, M. Beaudhuin, “Thermoelectric properties and stability of nanostructured chromium disilicide $CrSi_2$,” J. Appl. Phys. 126 (2019) 135103.
16. Z.J. Pan, L.T. Zhang, J.S. Wu, “Effects of Al doping on the transport performances of $CrSi_2$ single crystals,” Scripta Materialia 56 (2007) 245–248.
17. Z.J. Pan, L.T. Zhang, J.S. Wu, “Effects of V doping on the transport performances of $CrSi_2$ single crystals” Scripta Materialia 56 (2007) 257–260.

18. Y. Ohishi, A. Mohamad, Y. Miyazaki, H. Muta, K. Kurosaki, S. Yamanaka, “Thermoelectric properties of $Cr_{1-x}Mo_xSi_2$,” Journal of Physics and Chemistry of Solids 87 (2015) 153–157.
19. H. Nagai, T. Takamatsu, Y. Iijima, K. Hayashi, Y. Miyazaki, “Effects of Nb substitution on thermoelectric properties of $CrSi_2$,” Journal of Alloys and Compounds 687 (2016) 37–41.
20. Nakasawa, T. Takamatsu, Y Iijima, K. Hayashi, Y Miyazaki, “Thermoelectric Properties of Mo and Ge co-substituted $CrSi_2$,” Transactions of the Materials Research Society of Japan 43 (2) (2018) 85–91.
21. K. Ioroi, Y. Aono, X. Xu, T. Omori, R. Kainuma, J. Phase Equilib. Diffus. 43 (2022) 229–242.
22. S. Cui, I.-H. Jung, "Thermodynamic assessments of the Cr–Si and Al–Cr–Si systems," Journal of Alloys and Compounds 708 (2017) 887–902.
23. Y. Du, J.C. Schuster, "Experimental reinvestigation of the CrSi-Si partial system and update of the thermodynamic description of the entire Cr–Si system," J. Phase Equilibria 21 (3) (2000) 281–286.
24. Y.A. Chang, "Phase Relationships in the System Chromium-Silicon," Trans. Metall. Soc. AIME 242 (1968) 1509–1515.
25. V.N. Svechnikov, Y.A. Kocherzhinskii, L.M. Yupko, “Chromium-Silicon phase diagram,” Sb. Nauchn. Rab. Inst. Metallofiz. Akad. Nauk. Ukr. SSR 19 (1964) 212–218.
26. B.K. Voronov, L.D. Dudkin, N.I. Kiryukhina, N.N. Trusova, "Investigation of the Cr–Si system in the disilicide region," Sov. Powder Metall. Met. Ceram. 49 (1) (1967) 56–61.
27. L.B. Dubrovskaya, P.V. Gel'd, "Boundaries of the homogeneity region and nature of chromium disilicide," Russ. J. Inorg. Chem. 8 (7) (1963) 854–857.
28. L.D. Dudkin, E.S. Kuznetsova, "Investigation of the electrophysical properties of alloys based on semiconductor disilicides of chromium and manganese," Sov. Powder Metall. Met. Ceram. 12 (6) (1962) 20–31.

29. T.M. Pyatkova, V.I. Surikov, A.K. Shtolyts, V.L. Zagryazhskii, P.V. Gel'd, "β-Phase homogeneity region of a chromium-silicon system and mutual solubility of Cr_3Si and V_3Si," Izv. Akad. Nauk SSSR, Neorg. Mater. 7 (10) (1971) 1755–58.

30. M. Jurisch, G. Behr, "Growth and perfection of chromium-silicon (Cr_3Si) single crystals," Acta Phys. Acad. Sci. Hung. 47 (1979) 201–207.

31. R.G. Ross, W. Hume-Rothery, "High temperature X-ray metallography. I. A new debye-scherrer camera for use at very high temperatures II. A new parafocusing camera III. Applications to the study of chromium, hafnium, molybdenum, rhodium, ruthenium and tungsten," Journal of The Less-Common Metals, 5 (3) (1963) 258– 270.

32. R. Kieffer, F. Benesovsky, H. Schroth, "The system chromium-silicon and solid solutions of silicides," Z. Met. 44 (1953) 437–442.

33. C.H. Dauben, D.H. Templeton, C.E. Myers, "The crystal structure of Cr_5Si_3," J. Phys. Chem. 60 (1956) 443–445.

34. B. Boren, "X-ray study on alloys of silicon with chromium, manganese, cobalt and nickel," Arkiv. Kemi, Mineral. Geol. 11A (1933) 28.

35. T. Dasgupta, J. Etourneau, B. Chevalier, S.F. Matar, A.M. Umarji, "Structural, thermal, and electrical properties of $CrSi_2$," J. Appl. Phys. 103 (2008), 113516/113511-113516/113517.

36. W.M. Yim, R.J. Paff, "Thermal expansion of AlN, sapphire, and silicon," Journal of Applied Physics, 45 (3) (1974) 1456–1457.

37. P. Pfizenmaier, A.S. Ulrich, M.C. Galetz, U. Glatzel, "Determination of heat treatment parameters by experiments and CALPHAD for precipitate hardening of Cr-Alloys with Si, Ge and Mo," Intermetallics 116 (2020) 106636.

38. S.V. Meschel, O.J. Kleppa, "Standard enthalpies of formation of some 3d transition metal silicides by high temperature direct synthesis calorimetry," J. Alloys Compounds 267 (1998) 128–135.

435 39. V.N. Eremenko, G.M. Lukashenko, V.R. Sidorko, “Thermodynamic properties of Chromium Disilicide and Monosilicide,” Zh. Fiz. Khim. 45 (1971) 1996–1998.

40. V.N. Eremenko, G.M. Lukashenko, V.R. Sidorko, A.M. Khar’kova, “Thermodynamic properties of chromium silicides,” Porosh. Met. 12 (1972) 61–65.

41. G.M. Lukashenko, V.P. Sidorko, L.M. Yupko, “Thermodynamic properties of chromium
440 silicides,” Porosh. Met. Kiev. (1986) 73–76.

42. T.G. Chart, “Thermodynamic properties of the tungsten-silicon and chromium-silicon systems,” Met. Sci. 9 (1975) 504–509.

43. J.P. Riegert, A. Vermande, I. Ansara, “Thermodynamic properties of the mixture of the liquid chromium-silicon system at 1900 K,” High. Temp. - High. Press. 5 (1973) 231–237.

445 44. C.E. Myers, R.J. Kematick, G.A. Murray, “Thermodynamic activities, phase equilibria and stabilities in transition metal-silicon systems by high temperature Knudsen cell mass spectrometry,” in: Proceedings of International Conference on User Applications of Alloy Phase Diagrams (1987) 105–108.

45. Y.M. Golutvin, C.i.-K. Liang, “Heats of formation, heat contents, and heat capacities of
450 chromium silicides,” Zh. Fiz. Khim. 35 (1961) 129–141.

46. L. Topor, O.J. Kleppa, “Standard enthalpy of formation of chromium silicide of $CrSi_2$ by high-temperature mixing calorimetry,” J. Chem. Thermodynamics 19 (1987) 69–75.

47. Y.O. Esin, P.V. Gel’d, Y.V. Gorbunov, V.I. Vasil’ev, A.B. Galeznik, “Enthalpies of formation of molten chromium-silicon alloys,” Zh. Fiz. Khim. 50 (1976) 2656–2657.

455 48. G.I. Kalishevich, P.V. Gel’d, R.P. Krentsis, “Standard heat capacities, entropies, and enthalpies of silicon, chromium, and chromium silicides,” Zh. Fiz. Khim. 39 (1965) 2999–3001.

49. G.I. Kalishevich, P.V. Gel’d, R.P. Krentsis, “Specific heat, enthalpy, and entropy of Cr_5Si_3 and $CrSi_2$,” Teplofiz. Vys. Temp. 4 (1966) 653–659.

50. G.I. Kalishevich, P.V. Gel’d, Y.V. Putintsev, “Heat capacity, enthalpy, and entropy of chromium
460 and nickel monosilicides,” Tr. Ural. Politekh. Inst. 167 (1968) 152–154.

51. V.M. Pan, A.D. Shevchenko, I.G. Mikhailov, V.E. Yachmenev, G. Behr, “Heat capacity of chromium-silicon (Cr_3Si) single crystals in the temperature range 6–300 K,” Fiz. Nizk. Temp. Kiev. 6 (1980) 236–239.

52. V.I. Surikov, G.I. Kalishevich, P.V. Gel’d, “Thermodynamic characteristics of chromium-silicon (Cr_3Si), chromium-germanium (Cr_3Ge), vanadium-silicon (V_3Si), and vanadium-germanium (V_3Ge) compounds,” Zh. Fiz. Khim. 49 (1975) 555–556.

53. C.A. Coughanowr, I. Ansara, "Assessment of the Cr–Si system," Calphad 18 (2) (1994) 125–140.

54. H. Chen, Y. Du, J.C. Schuster, "On the melting of Cr_5Si_3 and update of the thermodynamic description of Cr–Si,” Calphad 33 (1) (2009) 211–214.

55. A.T. Dinsdale, “SGTE data for pure elements,” Calphad 15 (4) (1991) 317–425.

56. W. Xiong, M. Selleby, Q. Chen, J. Odqvist, Y. Du, “Phase equilibria and thermodynamic properties in the Fe-Cr system,” Critical Reviews in Solid State and Materials Sciences 35 (2) (2010) 125–152.

57. R. Hultgren, P.D, Desai, D. Hawkins, M. Gleiser, K. Kelley, “Selected values of the thermodynamic properties of the elements,” National Standard Reference Data System (1973) Tech. rep.

58. H. Okamoto, M. Schlesinger, E. Mueller, “Asm Handbook Volume 3: Alloy phase diagrams,” Ohio: Asm International (1992).

59. E. Rudy, St. Windisch, “The phase diagrams hafnium-vanadium and hafnium-chromium,” Journal of the Less-Common Metals 15 (1) (1968) 13–27.

60. D. Josell, D. Basak, J.L. McClure, U.R. Kattner, M.E. Williams, W.J. Boettinger, M. Rappaz, “Moving the pulsed heating technique beyond monolithic specimens: Experiments with coated wires,” (2001) Journal of Materials Research 16 (8) (2001) 2421–2428.

61. O. Redlich, A.T. Kister, “Thermodynamics of nonelectrolytic solutions. Algebraic representation of thermodynamic properties and the classification of solutions,” Ind. Eng. Chem. 40 (2) (1948) 345–348.

62. G. Inden, Report of the project meeting CALPHAD V. Ch. (Düsseldorf, Max Planck Institut Eisenforsch.) 111 (4) (1976) 1–13.

63. G. Inden, Physica 103B (1981) 82–100.

64. M. Hillert, M. Jarl, “A Model for Alloying Effects in Ferromagnetic Metals,” CALPHAD 2(3) (1978) 227–238.

65. M. Hillert, “The compound energy formalism,” J. Alloys Compd. 320 (2001) 161–176.

66. G. Kresse, J. Furthmüller, “Efficiency of ab-initio total energy calculations for metals and semiconductors using a plane-wave basis set,” Comp. Mat. Sci. 6 (1) (1996) 15–50.

67. G. Kresse, J. Furthmüller, “Efficient iterative schemes for ab initio total-energy calculations using a plane-wave basis set,” Phys. Rev. B 54 (16) (1996) 11169–11186.

68. P.E. Blöchl, “Projector augmented-wave method,” Phys. Rev. B 50 (24) (1994) 17953–17979.

69. J.P. Perdew, K. Burke, M. Ernzerhof, “Generalized Gradient Approximation Made Simple,” Physical Review Letters 77 (18) (1996) 3865–3868.

70. E. Fawcett, “Spin-density-wave antiferromagnetism in chromium,” Rev. Mod. Phys. 60 (1988) 209–283.

71. S. Asano, J. Yamashita, “Band Theory of Antiferromagnetic Chromium,” J. Phys. Soc. Jpn. 23 (4) (1967) 714–736.

72. P.E. Blöchl, O. Jepsen, O.K. Andersen, “Improved tetrahedron method for brillouin-zone integrations,” Phys. Rev. B 49 (23) (1994) 16223–16233.

73. B. Sundman, B. Jansson, J.-O. Andersson, “The Thermo-Calc Databank System,” Calphad 9 (2) (1985) 153–190.

74. Y. Pan, D.L. Pu, E.D. Yu, “Structural, electronic, mechanical and thermodynamic properties of Cr–Si binary silicides from first-principles investigations,” Vacuum 185 (2021) 110024.

75. Y. Pan, “Structural Prediction and Overall Performances of $CrSi_2$ Disilicides: DFT Investigations,” ACS Sustainable Chem. Eng. 8 (2020) 11024–11030.

76. B. Ren, D.-H. Lu, R. Zhou, D.-P. Ji, M.-Y. Hu, J. Feng, “First principles study of stability, mechanical, and electronic properties of chromium silicides,” Chin. Phys. B 27 (10) (2018) 107102.

515

Captions

Table 1 Summary of crystal structure information in the Cr–Si system.

Table 2 Lattice stability functions of the liquid and bcc phases of pure Cr.

Table 3 Formation energies of the A15 (Cr_3Si), Cr_5Si_3, CrSi, and $CrSi_2$ structures calculated using
520 first-principles calculations in this study and values from the literature [74,76].

Table 4 Summary of the optimized thermodynamic parameters for the Cr–Si binary system.

Table 5 Summary of the invariant reaction temperatures in the Cr–Si binary system.

Fig. 1 Cr–Si phase diagram calculated by Cui [22] compared with experimental data.

Fig. 2 Calculated thermodynamic properties of pure Cr: (a) specific heat (C_p); (b) molar enthalpy
525 (H_T-$H_{298.15}$); (c) molar entropy (S_m); and (d) molar Gibbs energy (G_m).

Fig. 3 Cr–Si phase diagram calculated in the present study compared with experimental data.

Fig. 4 Enlarged sections of Cr–Si phase diagram calculated in the present study focused on (a) the melting point of pure Cr, (b) the eutectic reaction of Liquid = Cr_3Si + Cr_5Si_3, and (c) the solubility composition ranges of the Cr_3Si and Cr_5Si_3 phases.

530 Fig. 5 Calculated enthalpy of formation of compounds in the Cr–Si binary system at 298.15 K compared with experimental data.

Fig. 6 Calculated enthalpy of mixing of the Cr–Si liquid phase at 1723 °C compared with experimental data.

Fig. 7 Calculated chemical potential diagrams of (a) Cr and (b) Si compared with experimental
535 data.

Fig. 8 Calculated specific heats of Cr-Si compounds, (a) Cr_3Si, (b) Cr_5Si_3, (c) CrSi, and (d) $CrSi_2$, compared with experimental data.

540 Table 1

Phase	Space group	System	Prototype	Pearson symbol	Lattice parameters / nm			Ref.
					a	b	c	
(Cr)	$Im\bar{3}m$	Cubic	W	cI2	0.2910	-	-	[31]
Cr_3Si	$Pm\bar{3}n$	Cubic	Cr_3Si	cP8	0.45580	-	-	[30] [32]
Cr_5Si_3	$I4/mcm$	Tetragonal	W_5Si_3	tI38	0.9170	0.4636	-	[33]
CrSi	$P2_13$	Cubic	FeSi	cP8	0.4620	-	-	[34]
$CrSi_2$	$P6_222$	Hexagonal	$CrSi_2$	hP9	0.442758	-	0.636805	[35]
(Si)	$Fd\bar{3}m$	Diamond	C	cF8	0.54309	-	-	[36]

Table 2

545

Symbol	Thermodynamic parameters / J·mol^{-1}	Temperature range / K
GHSERCR (SGTE)	$-8856.94 + 157.48\,T - 26.908\,T\ln T + 0.00189435\,T^2$ $-1.47721\times10^{-6}\,T^3 + 139250\,T^{-1}$	$298.15 < T < 2180$
${}^{\mathrm{SGTE}}G_{\mathrm{m}}^{\mathrm{bcc-Cr}}$	$-34869.344 + 344.18\,T - 50\,T\ln T$ $-2.88526\times10^{32}\,T^{-9}$	$2180 < T < 6000$
GLIQCR (SGTE)	GHSERCR $+ 24339.955 - 11.420225\,T$ $+2.37615\times10^{-21}\,T^7$	$298.15 < T < 2180$
${}^{\mathrm{SGTE}}G_{\mathrm{m}}^{\mathrm{liq.-Cr}}$	$-16459.984 + 335.616316\,T - 50\,T\ln T$	$2180 < T < 6000$
GHSERCR (This work)	$-8856.94 + 157.48\,T - 26.908\,T\ln T + 0.00189435\,T^2$ $-1.47721\times10^{-6}\,T^3 + 139250\,T^{-1}$	$298.15 < T < 2134$
$G_{\mathrm{m}}^{\mathrm{bcc-Cr}}$	$-35756.51223 + 344.55017\,T - 50\,T\ln T$ $-1.98572\times10^{32}\,T^{-9}$	$2134 < T < 6000$
GLIQCR (This work)	GHSERCR $+ 23793.7677 - 11.367098\,T$ $+2.300386\times10^{-21}\,T^7$	$298.15 < T < 2134$
$G_{\mathrm{m}}^{\mathrm{liq.-Cr}}$	$-16908.0241 + 335.616316\,T - 50\,T\ln T$	$2134 < T < 6000$

Table 3

Crystal structure	Composition	Formation enthalpy at 0 K (DFT) / kJ·mol^{-1}					
		This work	Reports		Open database *		
			Pan [74, 75]	Ren [76]	OQMD	MP	AFLOW
A15 (Cr_3Si)	Cr_3Si	−33.10	−33.45	−34.25	-34.93	-13.70	-34.16
	Cr_3Cr	7.63	-	-	5.69	34.54	-
Cr_5Si_3	Cr_5Si_3	−29.91	−30.20	−30.30	-30.01	-11.77	-30.78
	Si_5Si_3	51.01	-	-	-	-	-
B20 (CrSi)	CrSi	−28.16	−28.94	−29.14	-27.79	-13.70	-28.85
C40 ($CrSi_2$)	$CrSi_2$	−34.68	−36.61	−27.40	-34.73	-23.54	-35.22

* OQMD = Open Quantum Materials Database, MP = Materials Project, AFLOW = Automatic FLOW for Materials Discovery

550

Table 4

Phase: Model	Thermodynamic parameters / J·mol^{-1}	
Liquid: (Cr, Si)	${}^{0}L_{\mathrm{Cr,Si}}$ =	$-133515.58 + 21.8557\ T$
	${}^{1}L_{\mathrm{Cr,Si}}$ =	$-51796.75 + 20.3428\ T$
	${}^{2}L_{\mathrm{Cr,Si}}$ =	+17482.89
BCC_A2: (Cr, Si)(Va)	${}^{0}L_{\mathrm{Cr,Si:Va}}$ =	$-145125.11 + 26.6178\ T$
	${}^{1}L_{\mathrm{Cr,Si:Va}}$ =	$-5472.77 + 1.8645\ T$
	${}^{2}L_{\mathrm{Cr,Si:Va}}$ =	+5609.13
Cr_3Si: $(Cr)_3(Cr,Si)$	${}^{o}G_{\mathrm{Cr:Cr}}$ =	+24800.00 + 4 × GHSERCR
	${}^{o}G_{\mathrm{Cr:Si}}$ =	$-136659.01 + 11.9521\ T$ + 3 × GHSERCR + GHSERSI
	${}^{0}L_{*:\mathrm{Cr,Si}}$ =	$+19815.27 - 14.9873\ T$
Cr_5Si_3: $(Cr,Si)_5(Si)_3$	${}^{o}G_{\mathrm{Cr:Si}}$ =	$-343029.71 + 1316.1078\ T$ $-220.2616\ T\ ln\ T + 0.0133976\ T^2$ $-8.6238\times10^{-6}\ T^3 + 1.310080\times10^{6}\ T^{-1}$ (298.15 < T/K < 1963) $-549661.59 + 2522.5827\ T - 366.3668\ T\ ln\ T$ (1963 < T/K < 6000)
	${}^{o}G_{\mathrm{Si:Si}}$ =	+408051.46 + 8 × GHSERSI
	${}^{0}L_{\mathrm{Cr,Si:*}}$ =	$+603001.85 - 594.4585\ T$
CrSi: (Cr)(Si)	${}^{o}G_{\mathrm{Cr:Si}}$ =	$-79807.98 + 310.9269\ T - 51.6287\ T\ ln\ T$ $-0.0044736\ T^2 + 391330\ T^{-1}$
$CrSi_2$: (Cr)$(Si)_2$	${}^{o}G_{\mathrm{Cr:Si}}$ =	$-103372.31 + 388.9230\ T - 65.6523\ T\ ln\ T$ $-0.0114828\ T^2 - 1.7786\times10^{-9}\ T^3$ $+365454\ T^{-1}$

* The unit of mole is one formula unit for Cr_3Si, Cr_5Si_3, CrSi and $CrSi_2$ phases, one atom for liquid and bcc-Cr solid solution phases.

555 Table 5

Reaction type	Invariant reaction	Exp. / °C	Cal. / °C	Dev. / °C
Eutectic	Liquid = (Cr) + Cr_3Si	1715	1720	+5
Eutectic	Liquid = Cr_3Si + Cr_5Si_3	1665	1670	+5
Peritectic	Liquid + Cr_5Si_3 = CrSi	1442	1438	−4
Eutectic	Liquid = CrSi + $CrSi_2$	1404	1412	+8
Eutectic	Liquid = $CrSi_2$ + (Si)	1329	1335	+8

* Exp. = Experimental data [21]; Cal. = Calphad; Dev. = Deviation between experimental data [21] and calphad.

Fig. 1

560

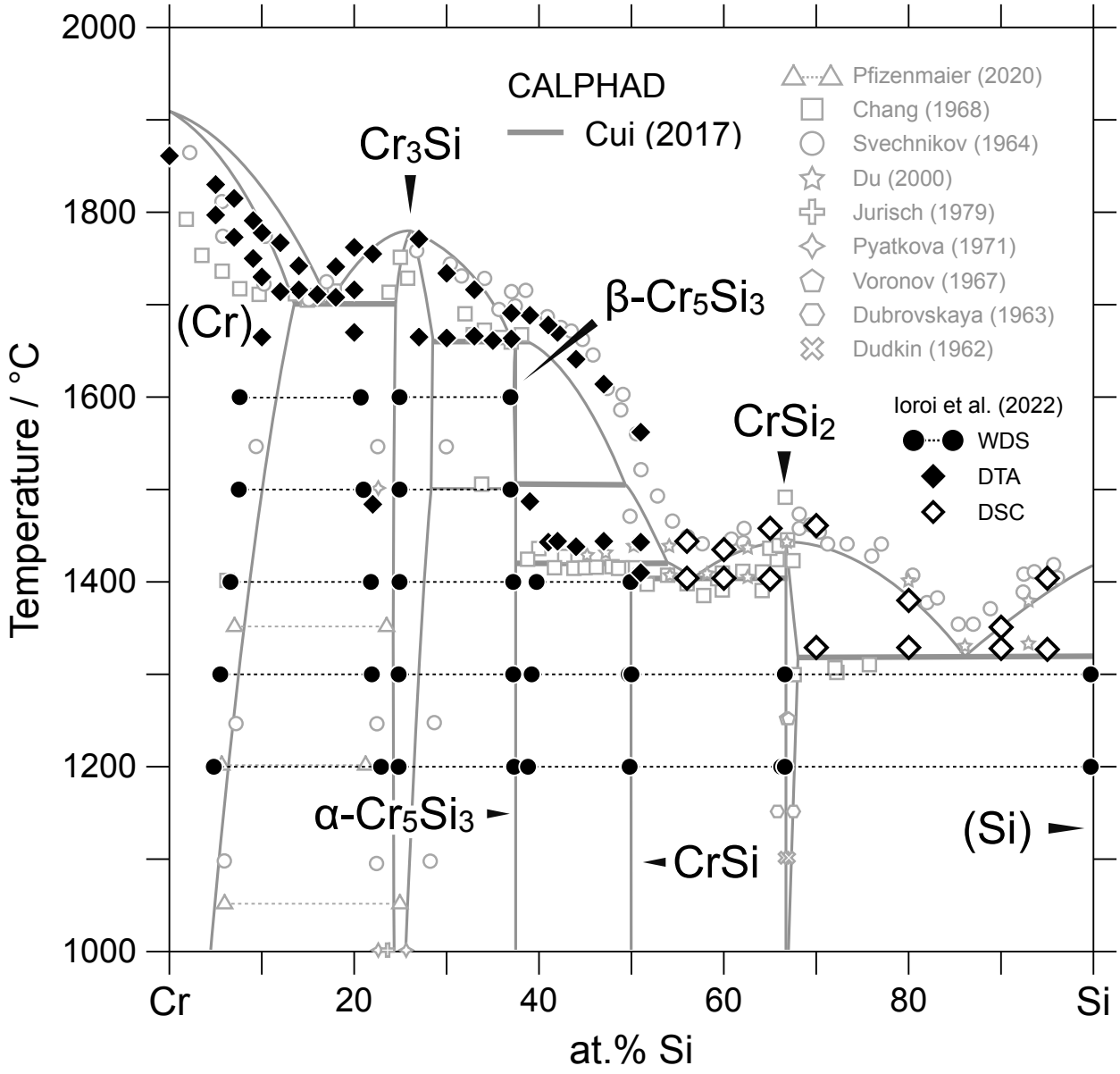
2000
1800
1600
1400
1200
1000
Temperature / °C
Cr
20
40
60
80
Si
at.% Si
CALPHAD
Cui (2017)
Cr3Si
(Cr)
β-Cr5Si3
CrSi2
α-Cr5Si3
CrSi
(Si)
Pfizenmaier (2020)
Chang (1968)
Svechnikov (1964)
Du (2000)
Jurisch (1979)
Pyatkova (1971)
Voronov (1967)
Dubrovskaya (1963)
Dudkin (1962)
Ioroi et al. (2022)
WDS
DTA
DSC

Fig. 2

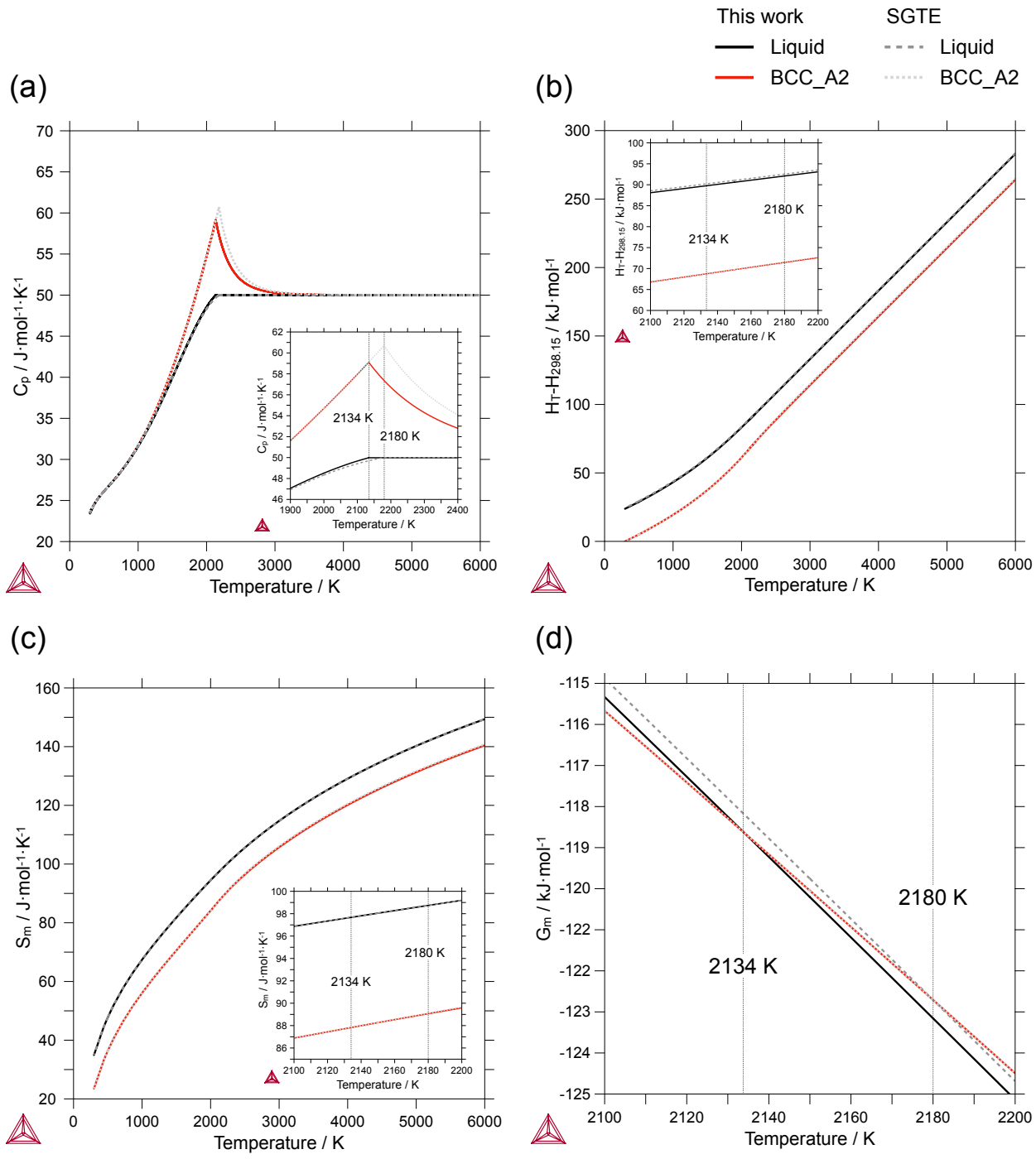
This work
Liquid
BCC_A2
SGTE
Liquid
BCC_A2
(a)
(b)
(c)
(d)
Cp / J·mol-1·K-1
HT-H298.15 / kJ·mol-1
Sm / J·mol-1·K-1
Gm / kJ·mol-1
Temperature / K
2134 K
2180 K

Fig. 3

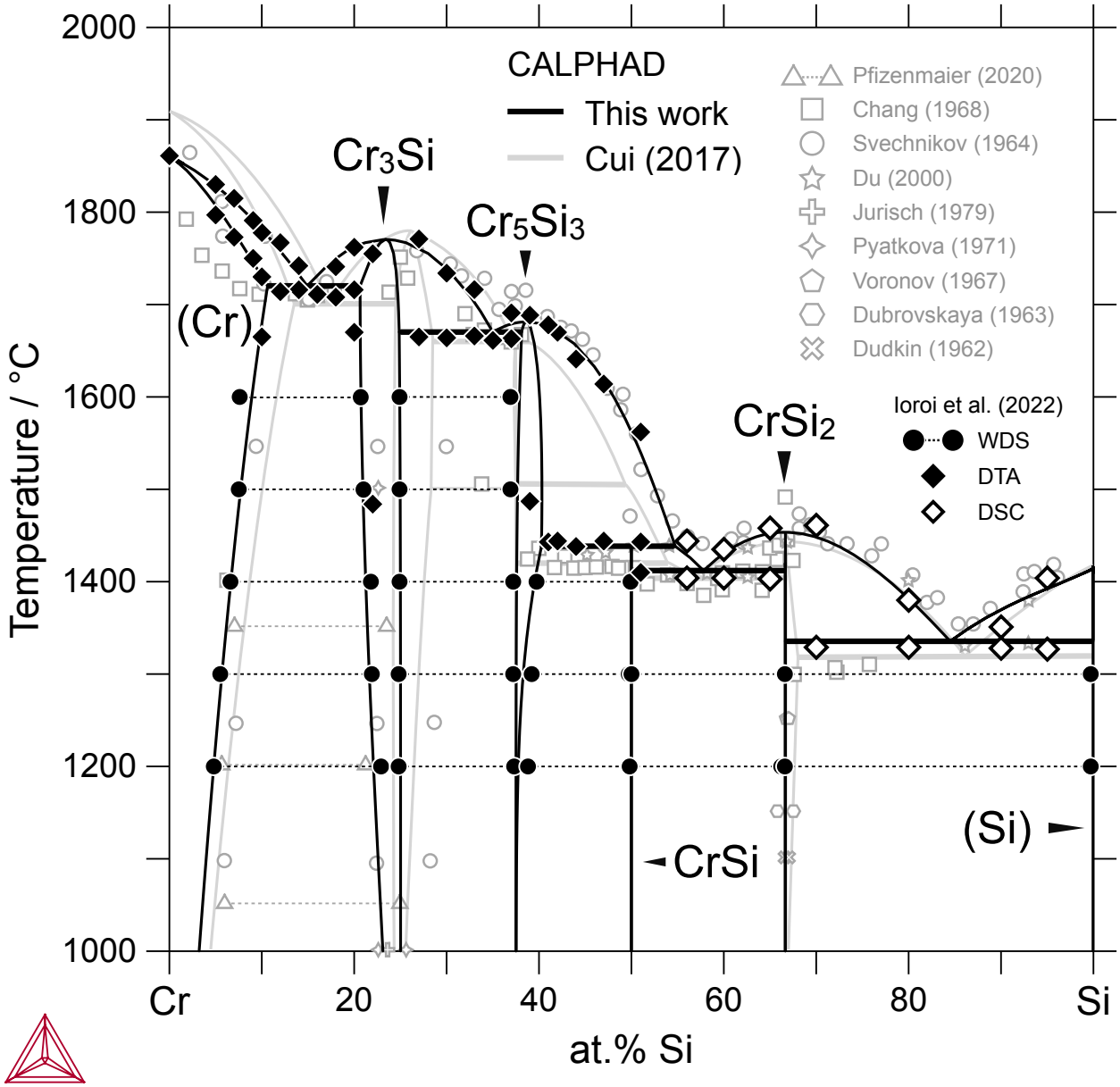
CALPHAD
This work
Cui (2017)
Pfizenmaier (2020)
Chang (1968)
Svechnikov (1964)
Du (2000)
Jurisch (1979)
Pyatkova (1971)
Voronov (1967)
Dubrovskaya (1963)
Dudkin (1962)
Ioroi et al. (2022)
WDS
DTA
DSC
Cr3Si
Cr5Si3
CrSi2
(Cr)
CrSi
(Si)
Temperature / °C
at.% Si
2000
1800
1600
1400
1200
1000
Cr
20
40
60
80
Si

565 Fig. 4

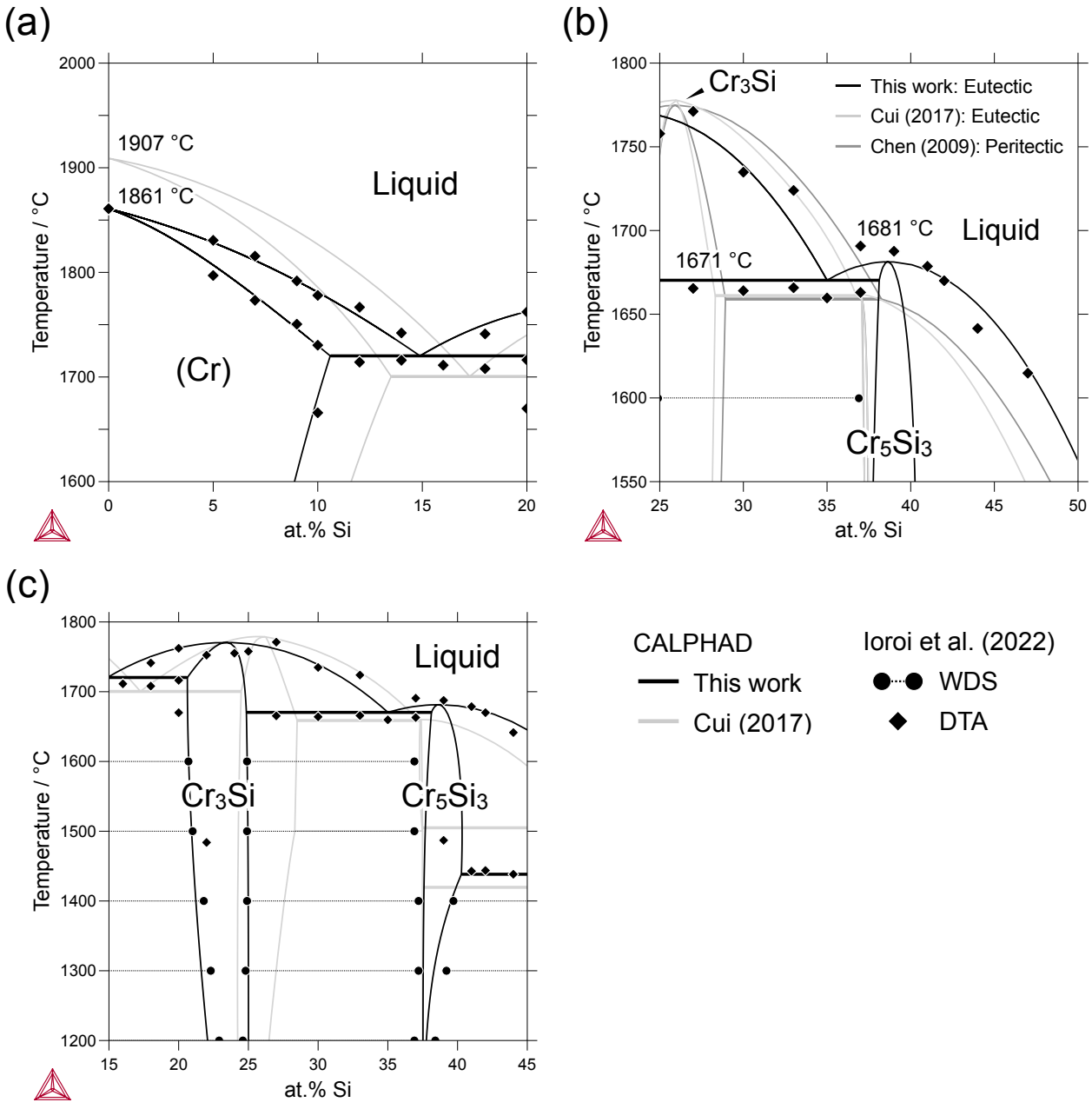
(a)
1907 °C
1861 °C
Liquid
(Cr)
Temperature / °C
at.% Si
(b)
Cr3Si
This work: Eutectic
Cui (2017): Eutectic
Chen (2009): Peritectic
1681 °C
Liquid
1671 °C
Cr5Si3
Temperature / °C
at.% Si
(c)
Liquid
Cr3Si
Cr5Si3
Temperature / °C
at.% Si
CALPHAD
This work
Cui (2017)
Ioroi et al. (2022)
WDS
DTA

Fig. 5

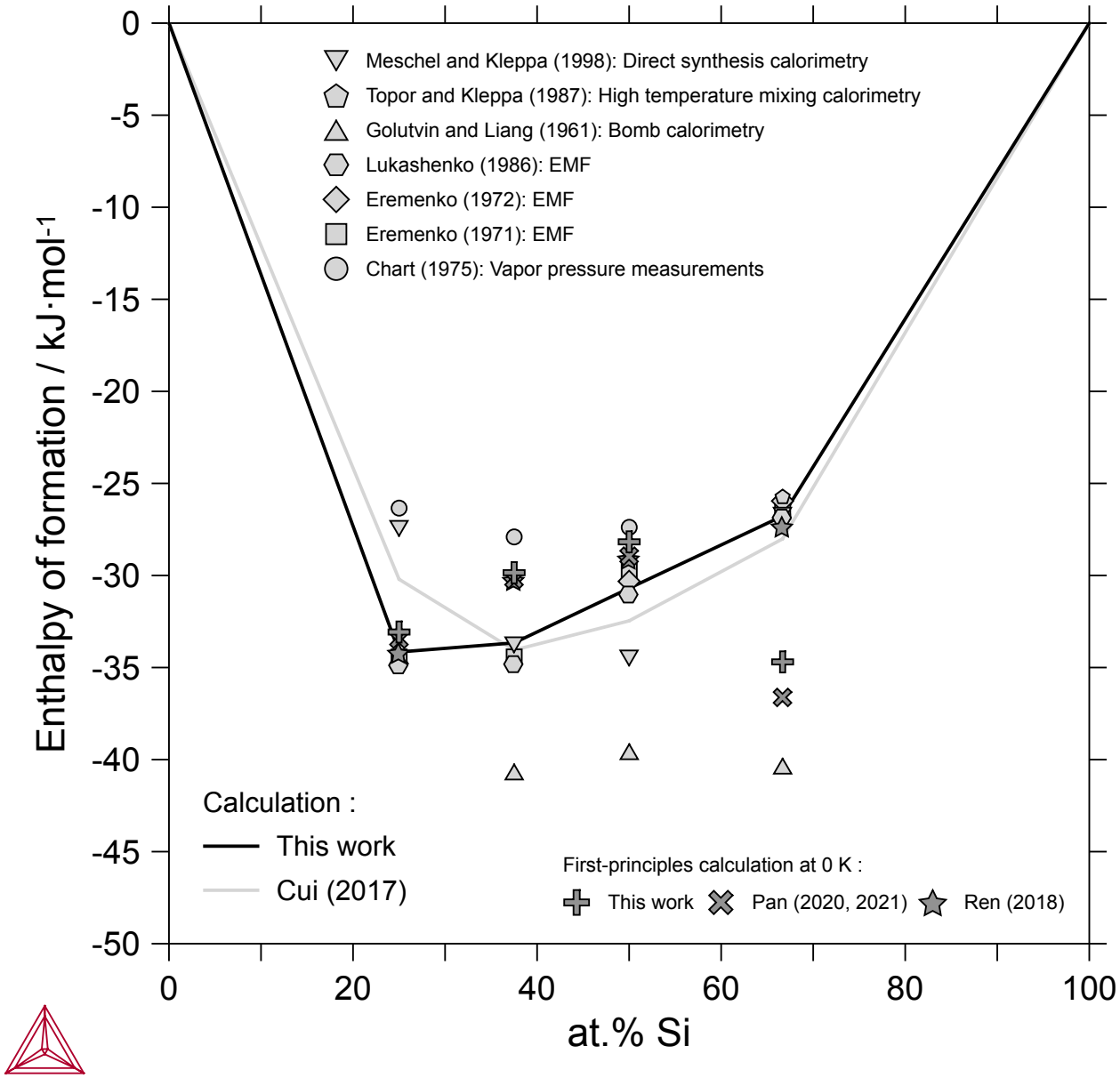
Meschel and Kleppa (1998): Direct synthesis calorimetry
Topor and Kleppa (1987): High temperature mixing calorimetry
Golutvin and Liang (1961): Bomb calorimetry
Lukashenko (1986): EMF
Eremenko (1972): EMF
Eremenko (1971): EMF
Chart (1975): Vapor pressure measurements
Calculation :
This work
Cui (2017)
First-principles calculation at 0 K :
This work
Pan (2020, 2021)
Ren (2018)
Enthalpy of formation / kJ·mol-1
at.% Si
0
-5
-10
-15
-20
-25
-30
-35
-40
-45
-50
0
20
40
60
80
100

Fig. 6

570

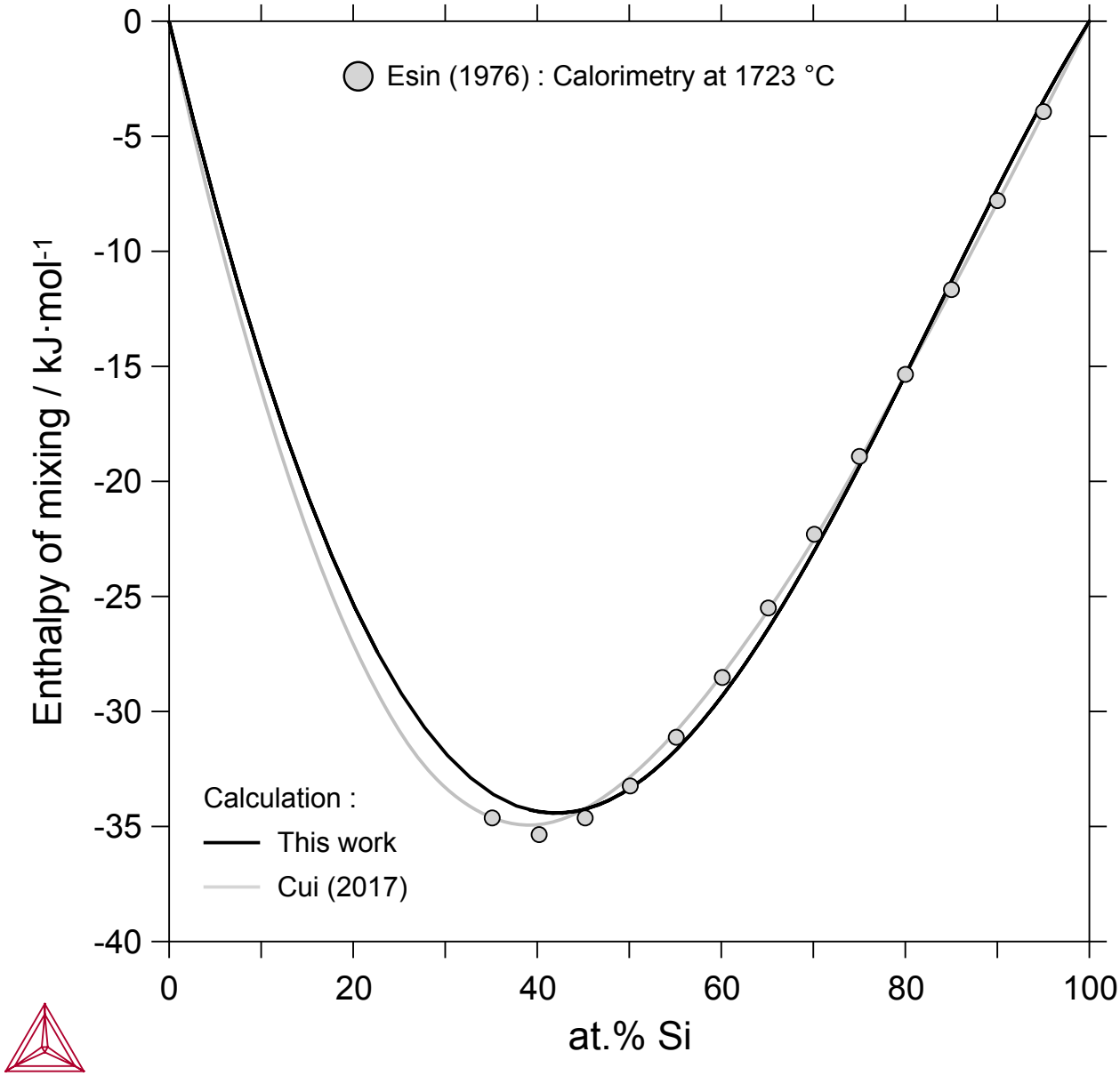
Esin (1976) : Calorimetry at 1723 °C
Calculation :
This work
Cui (2017)
Enthalpy of mixing / kJ·mol-1
at.% Si
0
-5
-10
-15
-20
-25
-30
-35
-40
0
20
40
60
80
100

Fig. 7

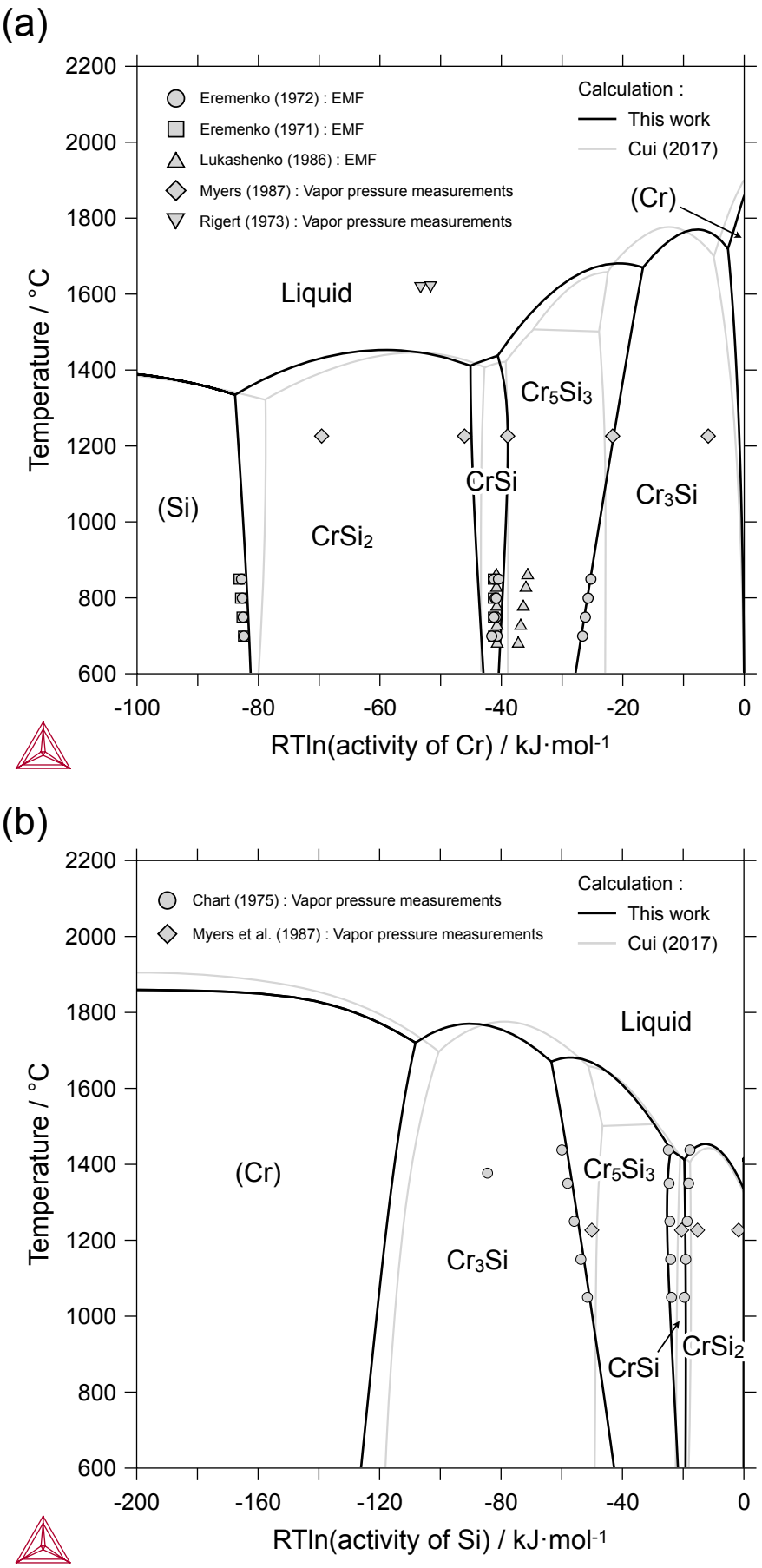
(a)
Eremenko (1972) : EMF
Eremenko (1971) : EMF
Lukashenko (1986) : EMF
Myers (1987) : Vapor pressure measurements
Rigert (1973) : Vapor pressure measurements
Calculation :
This work
Cui (2017)
(Cr)
Liquid
Cr5Si3
CrSi
Cr3Si
(Si)
CrSi2
Temperature / °C
RTln(activity of Cr) / kJ·mol-1
(b)
Chart (1975) : Vapor pressure measurements
Myers et al. (1987) : Vapor pressure measurements
Calculation :
This work
Cui (2017)
Liquid
(Cr)
Cr5Si3
Cr3Si
CrSi
CrSi2
Temperature / °C
RTln(activity of Si) / kJ·mol-1

Fig. 8

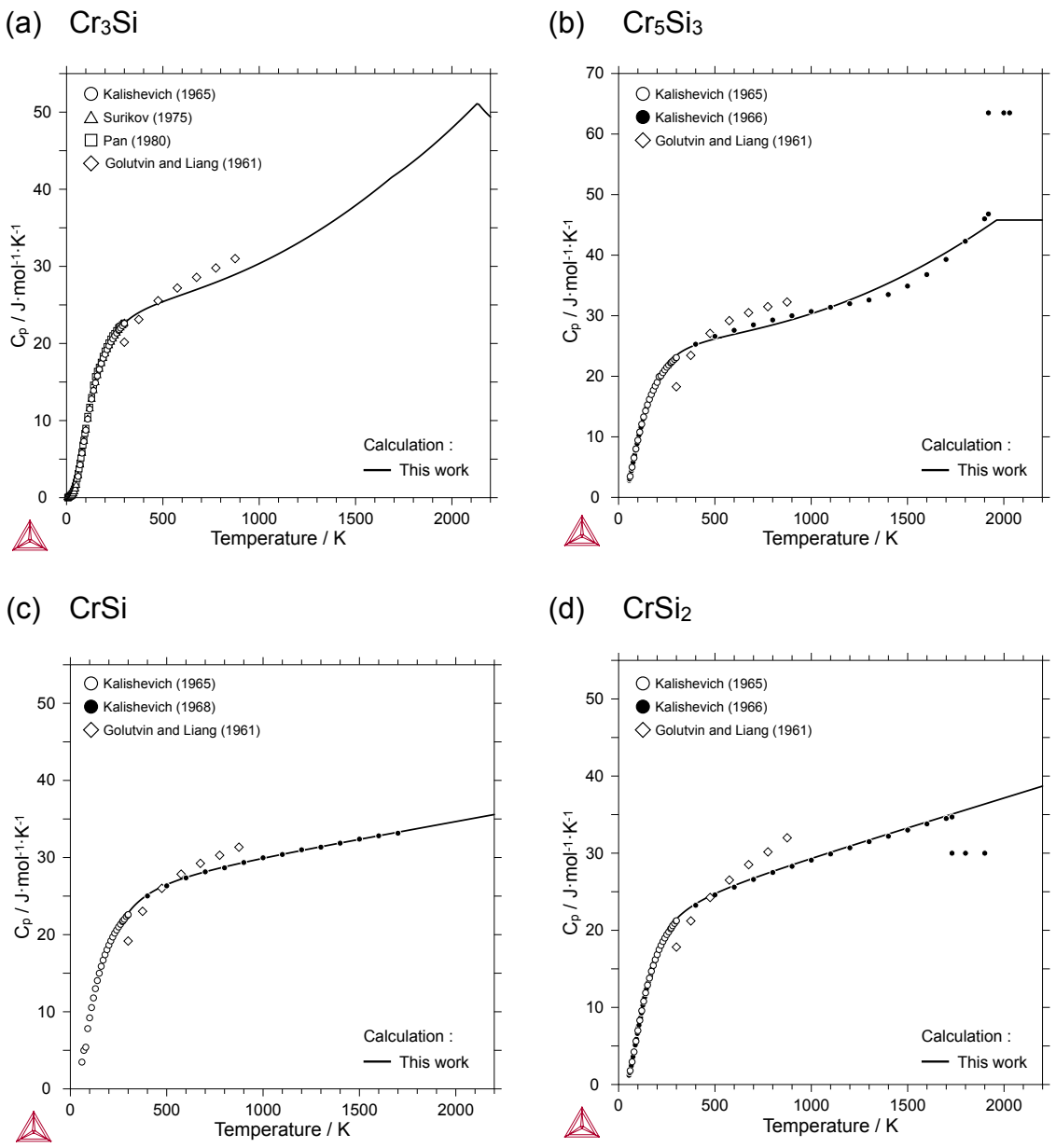
(a) Cr3Si
Kalishevich (1965)
Surikov (1975)
Pan (1980)
Golutvin and Liang (1961)
Calculation :
This work
Cp / J·mol-1·K-1
Temperature / K
(b) Cr5Si3
Kalishevich (1965)
Kalishevich (1966)
Golutvin and Liang (1961)
Calculation :
This work
Cp / J·mol-1·K-1
Temperature / K
(c) CrSi
Kalishevich (1965)
Kalishevich (1968)
Golutvin and Liang (1961)
Calculation :
This work
Cp / J·mol-1·K-1
Temperature / K
(d) CrSi2
Kalishevich (1965)
Kalishevich (1966)
Golutvin and Liang (1961)
Calculation :
This work
Cp / J·mol-1·K-1
Temperature / K